Polymer Degradation and Stability 94 (2009) 1267–1280

Contents lists available at ScienceDirect

Polymer Degradation and Stability

journal homepage: www.elsevier.com/locate/polydegstab

Thermal response to fire of a fibre-reinforced sandwich panel: Model formulation, selection of intrinsic properties and experimental validation

Antonio Galgano [a], Colomba Di Blasi [a,*], Carmen Branca [b], Eva Milella [c]

[a] Dipartimento di Ingegneria Chimica, Università degli Studi di Napoli "Federico II", P.le V. Tecchio, 80125 Napoli, Italy
[b] Istituto di Ricerche sulla Combustione, C.N.R., P.le V. Tecchio, 80125 Napoli, Italy
[c] IMAST SCarl, P.le E. Fermi, Granatello, 80055 Portici, Italy

ARTICLE INFO

Article history:
Received 29 December 2008
Received in revised form
3 April 2009
Accepted 6 April 2009
Available online 17 April 2009

Keywords:
Glass reinforced plastics
Sandwich panels
Mathematical modelling
Fire response

ABSTRACT

A predictive model is formulated for the fire response of a glass reinforced plastic panel, consisting of two glass-fibre/polyester skins and Vermiculux sandwich material (core) in between. Polymer conversion takes place according to a first-order decomposition reaction and an *n*-order combustion reaction both with an Arrhenius-type dependence on temperature. Intrinsic kinetic parameters have been estimated by re-examination of thermogravimetric data at four heating rates, resulting in activation energies for the two steps of 128 and 150 kJ/mol, respectively. Physical processes are modelled by the unsteady, one-dimensional conservation equations taking into account heat transfer by convection and conduction, convective mass transfer, surface heat transfer, effective thermal conductivity, moisture evaporation, ablation of the heat-exposed surface at a critical temperature and property variation. Simulated process dynamics, using intrinsic values for all the model parameters, are highly influenced by the behaviour of the heat-exposed skin which shows three main regimes: I) very rapid conversion of a thin surface layer (fast heating regime), II) slowing down of the conversion processes following the formation of a thick insulating fibre glass layer (slow heating regime) and III) a new enhancement in the reaction rates as a consequence of surface collapse and ablation (ablation regime). Good agreement is obtained for the predicted and measured temperatures for both a single skin composite plate and a sandwich panel loaded with a hydrocarbon flame.

1. Introduction

Composite polymeric materials are widely employed in structural applications. Fibre-reinforced composites present high weight-specific stiffness and strength and are therefore especially suited for the maritime, railway and aeronautical transportation industries [1]. Even higher stiffness-to-weight ratios are attained with sandwich elements in the form of panels [1–4]. These are commonly made of two thin and yet stiff face skins which are separated by a thick lightweight and compliant core. The skins are made using a variety of fibres and resins, such as glass, carbon and Kevlar fibres, phenolic resins, polyesters, vinyl esters and epoxies, while the core structure is made from polymeric foams, end grain balsa wood or aramid (nomex) honeycomb. The faces of the panel offer a high resistance to external bending loads while the core is especially suited for resistance to external and smoothly varying shear loads.

In addition to mechanical resistance, fire hazards associated with the release of large amounts of heat, smoke and toxic compounds from the decomposition and combustion of polymeric materials are of paramount importance for the structure and personnel safety. Significant effort has been devoted to characterize the fire behaviour of polymer composites including the development of mathematical models. In this regard predictive models, after experimental validation using standard fire test methods, can help in minimizing the number of tests required for material qualification [5]. Also, after a truly comprehension of the physical and chemical mechanisms controlling the fire under standard conditions, the models can be generalized for the predictions of realistic fire scenario, in this way supporting multi-disciplinary design of practical appliances and reducing expensive fire testing. Numerous predictive models have been proposed for the behaviour of composite polymeric materials under fire conditions [5–17], including the work carried out at the University of Berkeley (CA) and the production of an open core source computer model indicated as Gypro [18]. Reviews on the modelling of charring and non-charring solid degradation are also available [19–23]. The current state of the art indicates that

* Corresponding author. Tel.: +39 081 7682232; fax: +39 081 2391800.
E-mail address: diblasi@unina.it (C. Di Blasi).

0141-3910/$ – see front matter © 2009 Elsevier Ltd. All rights reserved.
doi:10.1016/j.polymdegradstab.2009.04.007

Nomenclature

A	pre-exponential factor [s^{-1}]
c	specific heat [J/kgK]
d	pore diameter [m]
E	activation energy [kJ/mol]
k	thermal conductivity [W/mK]
H	width of the square section of the sample [m]
h_1	global heat transfer coefficient at the hot face [W/m^2K]
h_2	global heat transfer coefficient at the cold face [W/m^2K]
h_L	global heat transfer coefficient at the lateral surfaces [W/m^2K]
M	molecular weight [kg/kmol]
n	reaction order
p	pressure [Pa]
Pr	Prandtl number
R	universal gas constant [kJ/molK]
Ra	Rayleigh number
S	specific surface [m^{-1}]
t	time [s]
T	temperature [K]
T_e	temperature of the external environment [K]
T_f	flame temperature [K]
u	velocity [m/s]
x	spatial coordinate [m]
Y	mass fraction
α	polymeric mass fraction (kinetic model)
ΔH	reaction heat [kJ/kg]
ε	volumetric fraction
λ	latent heat of water vaporization [kJ/kg]
ρ	density [kg/m^3]
σ	Stefan–Boltzmann constant [W/m^2K^4]
ψ	attenuation factor
%dev	mean square deviations

Subscripts

0	initial condition
a	air
ab	ablation
C	core
c	combustion
cr	critical value
cs	calcium silicate (Vermiculux)
d	decomposition
e	effective
f	glass fibres
G	gaseous products of devolatilization and combustion
g	total gas and vapour
m	moisture
p	polymer
R	residue
S	skin
DTG	derivate thermogravimetry
TG	thermogravimetry
v	steam

predictive models essentially take into account convective and conductive heat transfer, in a few cases for variable volume media undergoing phase change with one- or multi-step decomposition mechanisms. Peculiar of this approach is the use of intrinsic chemical kinetics and physical properties of the composite taking into account the behaviour of the different compounds and their mass fractions observed from specific experiments different from those for the experimental validation of the entire model.

Contrary to predictive models which aim at a detailed description of each process in the governing equations for the thermal response of a composite material, empirical models have also been formulated. These commonly consider a simple heat conduction equation [24–28] with apparent (versus intrinsic) thermo-physical properties (heat capacity and thermal conductivity) which incorporate the effects of all the processes other than heat conduction. For instance, the apparent heat capacity takes into account the energetics of phase change, moisture evaporation and thermal decomposition, and is expressed in terms of an empirical function of the temperature (i.e. adiabatic calorimetry data [25] are generally proposed in the form of a correlation). Although there are advantages of the simple form of the equations, it is easily understandable that empirical models are sample specific and their usefulness and validity are extremely limited. In other words, equations for the apparent properties should be re-determined as sample conditions and properties (for example, percentages of the components in the composite material, initial moisture content, etc.) vary. In a few cases, empirical or semi-empirical models of thermochemical conversion of composite materials have also been extended to include simplified descriptions of structural effects. The state of the art in this sector is provided by the introduction section of Ref. [26] while a more recent effort is reported in [29,30].

Contrary to the case of composite materials, the more complicated configuration of sandwich panels exposed to fire has been considered only in one case [31]. More precisely, a glass reinforced plastic panel is modelled, consisting of two glass-fibre/polyester (GRP) skins and calcium silicate (Vermiculux) material in between, also simplified to a single skin panel [32–35]. The model of the sandwich panel [31] formally retains the main features of those already developed for composite materials. The external skin undergoes one-step decomposition kinetics, with guessed parameters, and one-dimensional transient heat transfer by convection and conduction. The core does not decompose and is interested only by heat conduction. Apparent specific heats take into account the enthalpy variations associated with moisture evaporation and polymer decomposition and empirical expressions are used for the thermal conductivities. Therefore, despite the innovative character of the study and the practical importance of the multi-layered system are undeniable, the model [31] is essentially empirical because of the simplifying assumptions made in the formulation of the model equations (i.e. the absence of convective heat and mass transport across the core) and the use of apparent property values chosen so as to obtain acceptable agreement between predicted and measured temperature profiles. The approach does not allow the model to be confidently applied for different experimental conditions or, more important, for materials other than those of the system under study by a simple modification in the values of the input parameters.

The general scope of the present study is to formulate a generalized transport model for sandwich panels under fire conditions which, in conjunction with experimental analysis, can be applied to evaluate the performances of new materials. Owing to the availability of experimental information, the same multi-layered structure employed in [31] is chosen. A dynamic model is formulated, by incorporating theoretically based sub-models for the

various processes and using intrinsic values for both chemical and physical properties, and experimentally validated.

2. Computer model

2.1. Problem formulation

The problem under study, schematized in Fig. 1, is a sandwich panel made from two thin skins separated by a thick core, that is, two glass-fibre/polyester skins and calcium silicate (Vermiculux) material in between, as in [31]. Thicknesses of the three zones are L_{S1}, L_{S2} and L_C, whereas the total width for the other two directions is H. The polymeric component is isophthalic polyester while, as in [36], Vermiculux "is a low-density calcium silicate board containing vermiculite and reinforced with selected fibres and fillers."

The panel is exposed to a hydrocarbon flame which produces a heat flux uniform in the plane of the panel so that the assumption of one-dimensional system along the panel thickness can be made. Given the complicated character of the thermal response of a composite material, multi-layered structure exposed to fire conditions, the mathematical description also makes use of further assumptions:

1) the composite material forming the skins consists of the volumetric fractions ε_f (glass fibres), ε_p (polymer), ε_m (moisture), and ε_g (gas and/or vapors);
2) the core structure consists of the volumetric fractions ε_{cs} (calcium silicate or, more precisely, Vermiculux), ε_m (moisture), and ε_g (gas and/or vapors);
3) the effective density of each condensed-phase component of the panel, ρ_f (glass fibres), ρ_p (polymer), ρ_m (moisture), and ρ_{cs} (Vermiculux), is constant whereas the corresponding volumetric fraction varies to take into account chemical and physical transformations occurring during exposition to fire;
4) the total volume occupied by each skin does not change as a consequence of thermal decomposition and combustion of the polymeric resin;
5) the core does not shrink or swell and is chemically inert;
6) the gas pressure, p, inside the pores of the sandwich is constantly at the atmospheric value;
7) the solid, liquid and gas/vapor phases are in a local thermal equilibrium;
8) the transport by diffusion of volatile species is small with respect to that by convection;
9) the transport by convection and diffusion of the liquid-phase moisture is negligible;
10) the gas/vapor mixture obeys to the ideal gas law.

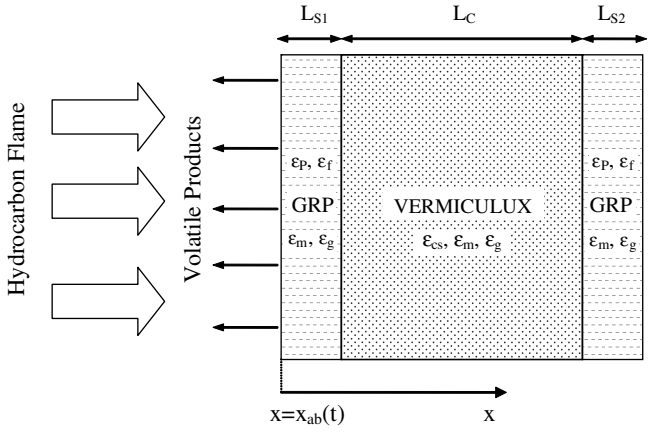

Fig. 1. Schematic of the GRP–Vermiculux sandwich panel.

Assumptions 1)–3) and 7)–10) are usually made in the formulation of transport equations for porous reacting solids [19–22]. The former group constitutes the basis of the so-called porous medium approximation, whereas the physical features supporting the others are the micro-porosity typical of the system under study (assumption 8)), the rather high gas velocities across the pores caused by the release of large amounts of decomposition/combustion products (assumption 8)), the rapid evaporation of the moisture content at temperatures near to the normal boiling point of water (assumption 9)) and the general validity of the ideal gas law (assumption 10)). As for the assumption 4), it is also well known [19] that the integrity of the structure shape is preserved for temperatures below the fibre glass fusion temperature which is much higher than the typical decomposition/combustion temperatures of polymeric resins. Assumption 5) is supported by the specific properties of the core material examined here. Finally, gas pressure variations taken into account by some models for the thermal decomposition of composite polymeric materials [7] and lignocellulosics [22] are reported not to play a controlling role for the thermal response.

However, the model takes into account the highly unsteady character of the process, thermal decomposition and combustion of the polymeric component of the skins both including finite-rate kinetics, heat transfer by convection and conduction (the latter with theoretically based sub-models for the effective thermal conductivities), convective mass transfer, variation of component volumetric fractions with the conversion degree, moisture evaporation, surface ablation of the solid residue left after the conversion of the polymeric resin as soon as the temperature reaches a critical value, heat transfer (convection and radiation) between the lateral and bottom surfaces of the sandwich panel and the environment, and variable properties. Sub-models are developed for the chemical and physical processes with intrinsic values for all the properties. Detailed information about the mathematical description of the various processes and a list of property values are provided below.

2.2. Oxidative decomposition kinetics of isophthalic polyester

Thermogravimetric curves for the oxidative decomposition (in air) of a pultruded E-glass fibre-reinforced polyester composite, where the polymer mass fraction is equal to 0.424, are reported in [28]. Given that the polymeric resin is isophthalic polyester, the same of the skins of the present system, they have been considered apt for the analysis of chemical kinetics needed for coupling with the description of transport phenomena of the model under development. First of all, the thermogravimetric curves, obtained at four heating rates (2.5, 5,10 and 20 K/min) from 298 to 973 K in air, have been re-plotted with reference to the sole polymeric component so as to get mass fractions in the range 0–1. They show a first high peak rate, attributable to thermal decomposition, followed by a much smaller peak associated with heterogeneous combustion. A mass fraction of unburned solid residue, α_r, around 0.05 can be detected. The two processes take place at approximately 500–700 K and 750–850 K, respectively.

The kinetic evaluations, proposed in [28], disregard the high-temperature combustion process and propose a simple one-step n-order reaction model. Evaluations of the integral data by means of the Ozawa method results in a pre-exponential factor $A = 4.53 \times 10^8\ s^{-1}$, an activation energy of $E = 125$ kJ/mol and a reaction

order $n = 2.75$. A more accurate, two-step mechanism is proposed here consisting of two parallel reactions attributable to decomposition and combustion:

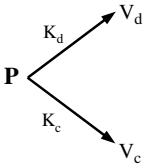

(P is the polymer and V_d and V_c are lumped classes of volatile products generated from decomposition and combustion, respectively). In accordance with the approach extensively used in the kinetic modelling of solid degradation [22], the active part of the solid is assumed to consist of two mass fractions, α_{d0} and α_{c0}, whose evolution is described by:

$$d\alpha_d/dt = -K_d\alpha_d, \quad (1)$$

$$\alpha_d(0) = \alpha_{d0}, \quad (2)$$

$$d\alpha_c/dt = -K_c\alpha_c^n, \quad (3)$$

$$\alpha_c(0) = \alpha_{c0}, \quad (4)$$

$$K_i = A_i \exp(-E_i/RT), \quad i = d, c \quad (5)$$

Then the overall mass loss rate is a linear combination of the two rates according to:

$$d\alpha/dt = d\alpha_d/dt + d\alpha_c/dt \quad (6)$$

The parameters α_{d0}, α_{c0}, A_d, A_c, E_d, E_c, and n should be estimated (for the total mass conservation, the following equation holds: $\alpha_r + \alpha_{d0} + \alpha_{c0} = 1$). The linear and the n-order dependence of the reaction rates on the mass fraction of volatiles released describe the volumetric and superficial (heterogeneous) character of the two processes, respectively [22,37]. The variation in the oxygen mass fraction, as a consequence of the combustion reaction, is assumed to be negligible. The method of parameter estimation employed here has already been presented elsewhere [16]. It makes use of a numerical solution for the mass conservation equations and a direct method for the minimization of the differential and integral form of the objective function taking simultaneously into account the differences between the model predictions and the experimental measurements for all the four heating rates data. The analysis leads to the kinetic parameters listed in Table 1. In particular, the decomposition reaction is responsible for a large part of solid devolatilization ($\alpha_{d0} = 0.88$) and is described by a pre-exponential factor and an activation energy that are quite close to those reported in [28], that is, $A_d = 4 \times 10^8$ s^{-1}, $E_d = 128$ kJ/mol. The combustion reaction is characterized by a higher value of activation energy (150 kJ/mol).

Simulations of the two component dynamics show that the two processes are in reality sequential, a feature that the general parallel mechanism proposed here can easily take into account. A good agreement between measurements and predictions is obtained as indicated by the curves shown in Fig. 2A and B and mean square deviations between predictions and measurements of about 2.5% and 4% for the integral and differential form of the curves, respectively. Although the introduction of an additional parameter with the assumption of an n-order rate also for the decomposition reaction could improve the agreement, especially at low temperatures, it has been preferred to preserve the adherence of the proposed model to the actual chemistry of the process. On the other hand, as the measured amount of volatiles released at low temperatures is very small, the complication does not seem necessary, for practical applications, of a further low-temperature decomposition step.

Fig. 3 provides a comparison, for a heating rate of 5 K/min, between the two-step kinetics proposed here and the one-step kinetics reported in [28] and that ($A = 7525$ s^{-1}, $E = 61$ kJ/mol, $n = 1$) coupled with the empirical transport models of GRP decomposition [31–33] (performances remain the same for the other heating rates). As already observed, the two-step kinetics shows very good agreement with measurements while the kinetics evaluated in [28] fails in the prediction of the position (585 K versus 606 K) and mainly the value (0.75×10^{-3} s^{-1} versus 1.3×10^{-3} s^{-1}) of the decomposition peak rate. A much larger disagreement is shown by the other set of kinetic parameters [31–33], characterized by a very low activation energy. Indeed, they highly anticipate the range of conversion temperatures, displaced at about 380–480 K (versus 500–850 K of the experimental data). Also, a lower peak rate is predicted (1×10^{-3} s^{-1} versus 1.3×10^{-3} s^{-1}).

Decomposition of polymeric materials in inert environment is also pertinent to the problem under study as, in the presence of gas

Table 1
Kinetic parameters and reaction enthalpies estimated for the two-step mechanism of isophthalic polyester decomposition and combustion.

A_d [s^{-1}] $= 4.0 \times 10^8$	E_d [kJ/mol] $= 128$	$\alpha_{d0} = 0.88$	ΔH_d [J/kg] $= 3.26 \times 10^6$
A_c [s^{-1}] $= 5.0 \times 10^7$	E_c [kJ/mol] $= 150$	$\alpha_{c0} = 0.07$	ΔH_c [J/kg] $= -9.217 \times 10^6$
$n = 0.85$	$\alpha_r = 0.05$	$\%dev_{TG} = 2.5$	$\%dev_{DTG} = 4$

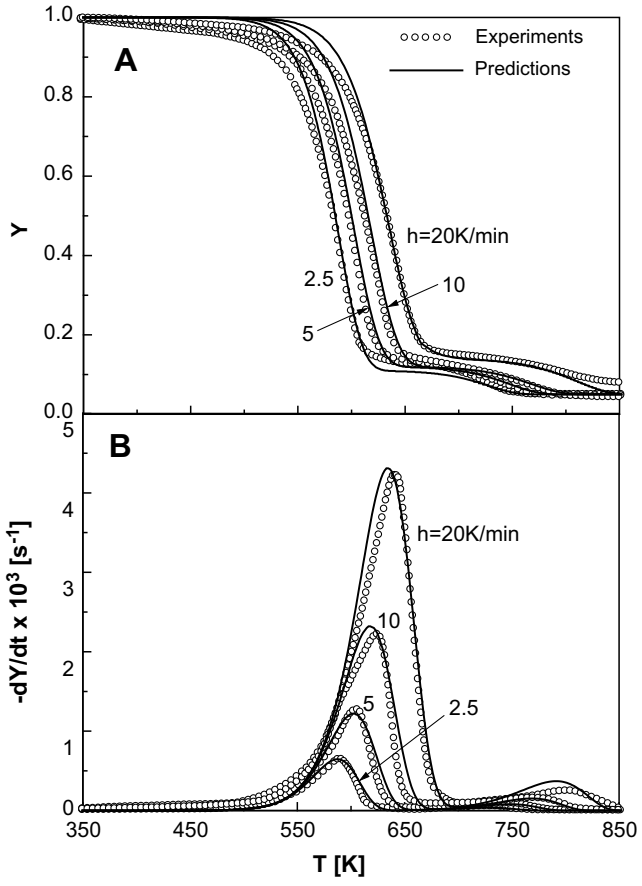

Fig. 2. (A, B) Comparison between the predictions (solid lines) of the two-step kinetic model (parameters in Table 1) and the measurements reported in [28] (symbols) for the mass fractions (A) and time derivatives of the mass fractions (B) of isophthalic polyester heated in air at 2.5, 5, 10 and 20 K/min.

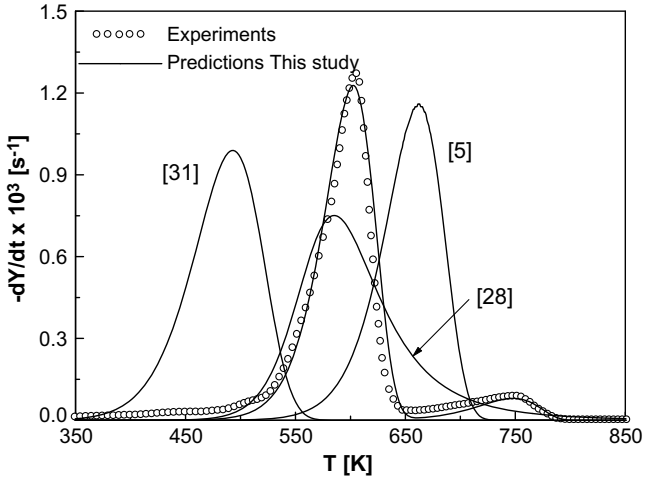

Fig. 3. Comparison between the predictions (solid lines) of the two-step kinetic model (parameters in Table 1), the one-step kinetics reported in [28] and [31] and the measurements [28] (symbols) for the time derivatives of the mass fraction of isophthalic polyester heated in air at 5 K/min. Results are also reported as obtained with the kinetics reported in [5] for the decomposition of isophthalic polyester in nitrogen.

phase combustion, the flame could act as a physical barrier for the oxygen to actually reach to solid surface. For the resin under study, thermogravimetric measurements in nitrogen for heating rates of 25–60 K/min and the parameters for a global one-step reaction ($A = 1.15 \times 10^8$ s^{-1}, $E = 134$ kJ/mol) are reported in [5]. A comparison of the decomposition kinetics in nitrogen and air (Fig. 3) shows that, in the former case, the process is displaced at higher temperatures but the peak rates are not significantly altered.

A few considerations should also be made in relation to the coupling of the kinetic model summarized in Table 1 with the transport equations for a sandwich panel exposed to fire conditions. As it is extensively discussed in the literature (see, for instance the recent review [22]) it is not possible to carry out kinetic analysis of solid fuel conversion for measurements carried out under very fast heating rates. Indeed, even for the small sample mass used in classical thermogravimetric analyzers, as soon as the external heating rate is increased, a significant temperature gradients is established across the sample, so that the control of the process shifts from the chemical reaction rate to the rate of internal heat transfer. Therefore, it is generally accepted that the error associated with the extrapolation at high heating rates, typical of practical applications, of the intrinsic kinetic data obtained at slow heating rates is certainly lower that that associated with the use of apparent kinetics, evaluated from experiments controlled by heat transfer.

For coupling with transport equations, the proposed kinetics needs the values of the reaction enthalpies to be specified. These, also reported in Table 1, are computed based on the following assumptions: a) the enthalpy of the one-step reaction reported in [33] (2.34×10^6 J/kg) is representative of the global energetics of the oxidative conversion process; and b) the enthalpy of the combustion reaction of the two-step mechanism coincides with that of carbon combustion (-9.217×10^6 J/kg [38]). From the two assumptions the enthalpy for the decomposition reaction of the two-step reaction mechanism can be easily computed ($(\alpha_{d0} + \alpha_{c0})2.34 \times 10^6$ J/kg $= \alpha_{d0}\Delta H_d + \alpha_{c0}\Delta H_c$, leading to $\Delta H_d = 3.26 \times 10^6$ J/kg).

2.3. Transport equations for the skins and the core

Transport equations should be formulated for the integration domain constituted by the skins ($x_{ab}(t) < x < L_{S1}$ and $L_{S1} + L_C < x < L_{S1} + L_C + L_{S2}$) and the core ($L_{S1} < x < L_{S1} + L_C$). The equations for the condensed-phase species of the two skins include two mass fractions of the resin, Y_d and Y_c, taking into account the evolution of volatiles from thermal decomposition and combustion (eqns. (7) and (8)), and a mass fraction for the liquid-phase moisture, Y_m (eqn. (9)):

$$\frac{d}{dt}Y_d = -\omega_d, \tag{7}$$

$$\frac{d}{dt}Y_c = -\omega_c, \tag{8}$$

$$\frac{d}{dt}Y_m = -\omega_m, \tag{9}$$

$$\omega_d = A_d \exp\left(-\frac{E_d}{RT}\right)Y_d, \tag{10}$$

$$\omega_c = A_c \exp\left(-\frac{E_c}{RT}\right)Y_c^n, \tag{11}$$

$$\omega_m = A_m \exp\left(-\frac{E_m}{RT}\right)Y_m. \tag{12}$$

The chemical reaction rates, ω_d and ω_c, are formulated in accordance with the two-step kinetics proposed above whereas the moisture evaporation rate, ω_m, is described following the treatment already used in several studies for the drying stage of porous solids [22]. It presents a linear dependence on the moisture mass fraction and an Arrhenius dependence on temperature.

Mass conservation equations for the gas phase should consider the presence of steam produced from moisture evaporation (ρ_v), air (ρ_a) which, for simplicity, is considered as a single species, and the gaseous products of the devolatilization and combustion reactions lumped again into one single species (ρ_G). More precisely, the equations are written for the conservation of steam (eqn. (13)) and the volatile products of chemical reactions (eqn. (14)) and the total gas/vapour continuity (eqn. (15)) together with the ideal gas law (eqn. (16)) and an algebraic equation for the total gas/vapour density (eqn. (17)) (the mean molecular weight of the gas/vapor phase mixture, M, and the total density of the skin, ρ_S, are given by eqns. (18) and (19)):

$$\frac{\partial}{\partial t}\varepsilon_g\rho_v - \frac{\partial}{\partial x}u\rho_v = \omega_m\rho_{S0}, \tag{13}$$

$$\frac{\partial}{\partial t}\varepsilon_g\rho_G - \frac{\partial}{\partial x}u\rho_G = (\omega_d + \omega_c)\rho_{S0}, \tag{14}$$

$$\frac{\partial}{\partial t}\varepsilon_g\rho_g - \frac{\partial}{\partial x}u\rho_g = (\omega_d + \omega_c + \omega_m)\rho_{S0}, \tag{15}$$

$$\rho_g = \frac{pM}{RT}, \tag{16}$$

$$\rho_g = \rho_a + \rho_G + \rho_v, \tag{17}$$

$$M = \frac{\rho_a M_a + \rho_G M_G + \rho_v M_v}{\rho_g}, \tag{18}$$

$$\rho_S = \varepsilon_m\rho_m + \varepsilon_p\rho_p + \varepsilon_f\rho_f + \varepsilon_g\rho_g. \tag{19}$$

The unsteady enthalpy conservation equation for the gas/vapor, solid and liquid phases (eqn. (20)) takes into account convective

and conductive transport, energetics of polymer degradation and combustion and moisture evaporation, and convective and radiative heat exchange across the lateral surface (the specific heat of the gas/vapour phase mixture, c_g, is given by eqn. (21)):

$$(\varepsilon_m\rho_m c_m + \varepsilon_p\rho_p c_p + \varepsilon_f\rho_f c_f + \varepsilon_g\rho_g c_g)\frac{\partial}{\partial t}T - u\rho_g c_g\frac{\partial}{\partial x}T = \frac{\partial}{\partial x}\left(k_e\frac{\partial}{\partial x}T\right) + \omega_d\rho_{S0}(-\Delta H_1) + \omega_c\rho_{S0}(-\Delta H_2) - \lambda\omega_m\rho_{S0} + S\left[h_L(T_e - T) + \sigma e\left(T_e^4 - T^4\right)\right], \quad (20)$$

$$c_g = \frac{\rho_a c_a + \rho_G c_G + \rho_v c_v}{\rho_g}, \quad (21)$$

where $S = 4/H$.

The mass conservation equations for the central core structure are written for the liquid-phase moisture (eqn. (22)), steam (eqn. (23)), volatile products of chemical reactions (eqn. (24)) and total gas/vapor-phase continuity (eqn. (25)), in conjunction with the ideal gas law (eqn. (26)) and an algebraic equation for the total gas/vapor-phase density (eqn. (27)) (the mean molecular weight of the gas/vapor phase mixture, M, and the total density of the core, ρ_C, are given by eqns. (28) and (29)):

$$\frac{d}{dt}Y_m = -\omega_m, \quad (22)$$

$$\frac{\partial}{\partial t}\varepsilon_g\rho_v - \frac{\partial}{\partial x}u\rho_v = \omega_m\rho_{C0}, \quad (23)$$

$$\frac{\partial}{\partial t}\varepsilon_g\rho_G - \frac{\partial}{\partial x}u\rho_G = 0, \quad (24)$$

$$\frac{\partial}{\partial t}\varepsilon_g\rho_g - \frac{\partial}{\partial x}u\rho_g = \omega_m\rho_{C0}, \quad (25)$$

$$\rho_g = \frac{pM}{RT}, \quad (26)$$

$$\rho_g = \rho_a + \rho_G + \rho_v, \quad (27)$$

$$M = \frac{\rho_a M_a + \rho_G M_G + \rho_v M_v}{\rho_g}, \quad (28)$$

$$\rho_C = \varepsilon_m\rho_m + \varepsilon_{cs}\rho_{cs} + \varepsilon_g\rho_g. \quad (29)$$

The enthalpy conservation equation (eqn. (30)) is expressed as (the specific heat of the gas/vapor phase mixture, c_g, is given by eqn. (31)):

$$(\varepsilon_m\rho_m c_m + \varepsilon_{cs}\rho_{cs}c_{cs} + \varepsilon_g\rho_g c_g)\frac{\partial}{\partial t}T - u\rho_g c_g\frac{\partial}{\partial x}T = \frac{\partial}{\partial x}\left(k_e\frac{\partial}{\partial x}T\right) - \lambda\omega_m\rho_{C0} + S\left[h_L(T_e - T) + \sigma e\left(T_e^4 - T^4\right)\right], \quad (30)$$

$$c_g = \frac{\rho_a c_a + \rho_G c_G + \rho_v c_v}{\rho_g}. \quad (31)$$

The transport equations for the core (eqns. (22)–(31)) are formally the same as already written for the skin layers except for the absence of chemical reactions and the different components.

The set of partial differential equations (eqns. (7)–(31)) can be used to predict the space and time variation of the dependent variables characterizing the state of the system (Y_d, Y_c, Y_m, ρ_v, ρ_G, ρ_g, u, T), after the specification of the initial and boundary conditions, the equations for the physical properties (volumetric mass fractions of the various components, specific heats, effective thermal conductivities, etc.) and the position $x_{ab}(t)$ of the heat-exposed surface.

2.4. Initial and boundary conditions

The sandwich panel is assumed to be initially at ambient conditions in air (T_0, ρ_{a0}) where the density of steam and volatile products is zero. Initial conditions should also be prescribed, on the basis of actual composition of the skin and core structure, for the mass fractions of the resin, Y_{d0} and Y_{c0}, and the moisture content, Y_{m0}.

Ordinary differential equations for the mass conservation of condensed-phase species (eqns. (7)–(9), (22)) do not require any boundary condition. The mass conservation equations for the gas/vapor phase species, given the assumption of negligible diffusion, are characterized by first-order spatial derivatives (convection). Therefore boundary conditions should be specified for the densities of steam (eqn. (32)) and volatile products of chemical reactions (eqn. (33)) and total gas/vapor mass flux (eqn. (34)) only at the bottom of the lower skin ($x = L_{S1} + L_C + L_{S2}$)

$$\rho_v|_{x=L_{S1}+L_C+L_{S2}} = 0, \quad (32)$$

$$\rho_G|_{x=L_{S1}+L_C+L_{S2}} = 0, \quad (33)$$

$$\rho_g u|_{x=L_{S1}+L_C+L_{S2}} = 0 \quad (34)$$

and at the skin/core interfaces ($x = L_{S1}$ and $x = L_{S1} + L_C$):

$$\rho_v|_{x=L_{S1}^-} = \rho_v|_{x=L_{S1}^+}, \quad (35)$$

$$\rho_G|_{x=L_{S1}^-} = \rho_G|_{x=L_{S1}^+}, \quad (36)$$

$$\rho_g u|_{x=L_{S1}^-} = \rho_g u|_{x=L_{S1}^+}, \quad (37)$$

$$\rho_v|_{x=(L_{S1}+L_C)^-} = \rho_v|_{x=(L_{S1}+L_C)^+}, \quad (38)$$

$$\rho_G|_{x=(L_{S1}+L_C)^-} = \rho_G|_{x=(L_{S1}+L_C)^+}, \quad (39)$$

$$\rho_g u|_{x=L_{S1}^-} = \rho_g u|_{x=L_{S1}^+}. \quad (40)$$

Equations (32)–(34) essentially describe the condition of zero velocity at the back side of the sandwich panel, which is a consequence of the assumption of constant pressure with a gas flow directed towards the heat-exposed surface. The conditions at the skin/core interfaces express the continuity of the species density and total gas flux.

Boundary conditions should be assigned for the enthalpy conservation equations at the bottom of the lower skin ($x = L_{S1} + L_C + L_{S2}$):

$$-k_e\left.\frac{\partial T}{\partial x}\right|_{x=L_{S1}+L_C+L_{S2}} = \sigma e|_{x=L_{S1}+L_C+L_{S2}}\left(T^4\big|_{x=L_{S1}+L_C+L_{S2}} - T_e^4\right) + h_2\left(T|_{x=L_{S1}+L_C+L_{S2}} - T_e\right) \quad (41)$$

at the skin/core interfaces ($x = L_{S1}$ and $x = L_C + L_{S1}$):

$$T|_{x=L_{S1}^-} = T|_{x=L_{S1}^+}, \quad (42)$$

$$k_e \frac{\partial T}{\partial x}\Big|_{x=L_{S1}^-} = k_e \frac{\partial T}{\partial x}\Big|_{x=L_{S1}^+}, \tag{43}$$

$$T|_{x=(L_{S1}+L_C)^-} = T|_{x=(L_{S1}+L_C)^+}, \tag{44}$$

$$k_e \frac{\partial T}{\partial x}\Big|_{x=(L_{S1}+L_C)^-} = k_e \frac{\partial T}{\partial x}\Big|_{x=(L_{S1}+L_C)^+} \tag{45}$$

and the heat-exposed surface ($x = x_{ab}(t)$):

$$-k_e \frac{\partial T}{\partial x}\Big|_{x=x_0} = \psi \sigma e|_{x=x_0} \left(T_f^4 - T^4\Big|_{x=x_0}\right) + h_1 \left(T_f - T|_{x=x_0}\right). \tag{46}$$

The boundary condition (eqn. (41)) describes the radiative and convective heat transfer between the bottom side of the sandwich and the environment. The interface conditions (eqns. (42)–(45)) establish the continuity of temperature and heat flux. Finally, the boundary condition (eqn. (46)) is assigned at the heat-exposed surface ($x = x_{ab}(t)$) and describes convective and radiative heating from a flame at a temperature T_f (an attenuation factor, ψ, is introduced to take into account the absorption of the radiation by the gas/vapor phase). The surface undergoes an ablation process, in accordance with the experimental observation [19,25,26], with the complete collapse of the specimen when the glass fibres attain temperatures above 1103 K (softening temperature). In reality the problem under study is a moving boundary one where x_{ab} is a function of time and moves from the origin ($x = 0$) towards the bottom side of the upper skin with the same speed as that of the front $T = T_{cr}$, where T_{cr} is an assigned critical temperature value:

$$x_{ab}(t) = 0 \text{ for } T(0,T) \le T_{cr} \quad \text{and} \quad x_{ab}(t) = x(T_{cr}) \text{ for } T(0,t) > T_{cr}. \tag{47}$$

To facilitate the identification of the processes controlling the dynamics of the thermal response of the multi-layered composite system under study, in addition to the case of the panel sandwich already presented, the case of a single composite-material skin, exposed to the same thermal conditions, is also considered. The model equations for this simpler structure are the same as already presented for the skin with the sole variation in the boundary conditions at the bottom side where eqns. (35)–(37), (43) are substituted by:

$$\rho_v|_{x=L_{S1}} = 0, \tag{48}$$

$$\rho_G|_{x=L_{S1}} = 0, \tag{49}$$

$$\rho_g u\Big|_{x=L_{S1}} = 0, \tag{50}$$

$$-k_e \frac{\partial T}{\partial x}\Big|_{x=L_{S1}} = \sigma e|_{x=L_{S1}} \left(T^4\Big|_{x=L_{S1}} - T_e^4\right) + h_2 \left(T|_{x=L_{S1}} - T_e\right). \tag{51}$$

2.5. Physical properties

Similar to the kinetic constants, the sub-models and parameter values of physical properties, such as specific heat, thermal conductivity and heat transfer coefficients, to be used in conjunction with the transport equations, have been obtained from measurements available in the literature. The property equations are listed and discussed below while the parameter values are collected in Table 2. As anticipated, the system under study is the same as in [31], so that some basic properties (ρ_p, ρ_f, ε_f, ε_{g0}) are derived from this study.

Although the total volume occupied by each single skin and core remains unvaried as a consequence of the occurrence of moisture evaporation and chemical reactions, the volumetric fractions occupied by the polymeric resin (ε_p) and the moisture (ε_m) are assumed to diminish proportionally to the amount of volatile species produced with a corresponding increase in the volumetric fraction of the gas/vapor phase (the volumetric fraction occupied by the glass fibres is constant):

$$\varepsilon_p + \varepsilon_f + \varepsilon_m + \varepsilon_g = 1 \quad \text{(skin)}, \tag{52}$$

$$\varepsilon_{cs} + \varepsilon_m + \varepsilon_g = 1 \quad \text{(core)}, \tag{53}$$

$$\frac{\varepsilon_p}{\varepsilon_{p0}} = \frac{Y_d + Y_c + Y_r}{Y_{d0} + Y_{c0} + Y_r}, \tag{54}$$

$$\frac{\varepsilon_m}{\varepsilon_{m0}} = \frac{Y_m}{Y_{m0}}. \tag{55}$$

There is no specific information about these effects from the experimental observation. Nevertheless this assumption seems to be a reasonable one.

The effective thermal conductivity of the skin, k_{eS}, takes into account the combined contribution of the various components, k'_e, and that of radiation in the form already used in previous heat transfer models for porous media [22]:

$$k_e = k'_e + 4d \frac{\varepsilon_g}{1 - \varepsilon_g} \sigma e T^3, \tag{56}$$

where d is the pore diameter and e the emissivity which is a function of temperature [33]:

Table 2
Physical property values used for numerical simulation.

Parameter	Value	Reference
A_m	5.6×10^8 [s^{-1}]	[39]
c_a	1100 [J/kgK]	[40]
c_{cs}	950 [J/kgK]	[47]
c_f	840 [J/kgK]	[41]
c_G	2500 [J/kgK]	[40]
c_m	4200 [J/kgK]	[38]
c_p	2500 [J/kgK]	[28]
c_v	2100 [J/kgK]	[38]
d	3.0×10^{-4} (skin) [m]	[28]
	2.0×10^{-5} (core) [m]	[47]
E_m	88 [kJ/mol]	[39]
k_{cs}	0.77 [W/mK]	[47]
k_m	0.23 [W/mK]	[42]
k_p	0.31 [W/mK]	[28]
M_G	95 [kg/kmol]	[43]
M_a	29 [kg/kmol]	[38]
M_v	18 [kg/kmol]	[38]
ε_{cs}	0.172	[36,38]
ε_f	0.465	[33]
ε_{g0}	0.15 (skin)	[35]
	0.773 (core)	[31,36,38]
ε_{m0}	0.018 (skin)	[31]
	0.055 (core)	
ε_{p0}	0.367	[33]
λ	2.26×10^6 [J/kg]	[38]
ρ_{cs}	2900 [kg/m^3]	[38]
ρ_f	2560 [kg/m^3]	[33]
ρ_p	1749 [kg/m^3]	[33]
ψ	0.7	[44]

$$e = 0.755 + 2.5 \times 10^{-4}(T - 293) \quad \text{for } T < 1273, \tag{57a}$$

$$e = 1.0 \quad \text{for } T = 1273. \tag{57b}$$

For the system polymer/gas/moisture on one side (k_{pgm}) and the glass fibres on the other (k_f), a series model is selected:

$$\frac{1}{k'_e} = \frac{\varepsilon_f}{k_f} + \frac{1 - \varepsilon_f}{k_{pgm}}. \tag{58}$$

The thermal conductivity of the system polymer/gas/moisture is described by a parallel mechanism where the component contribution is weighted in accordance with the corresponding volumetric fraction:

$$k_{pgm} = \frac{\varepsilon_P}{1 - \varepsilon_f} k_P + \frac{\varepsilon_g}{1 - \varepsilon_f} k_g + \frac{\varepsilon_m}{1 - \varepsilon_f} k_m. \tag{59}$$

The thermal conductivity of the gaseous mixture is a function of temperature [45]:

$$k_g = 9.00037 \times 10^{-3} + 5.6263 \times 10^{-5} T \quad [\text{W/mK}]. \tag{60}$$

A correlation for the glass fibre thermal conductivity on dependence of temperature is proposed, based on the measurements reported in [46] over the temperature range 300–1800 K, as shown in Fig. 4:

$$k_f = \frac{1.1 + 2.7 \times 10^{-17}(T - 293)^6}{1 + 7.0 \times 10^{-18}(T - 293)^6} \quad [\text{W/mK}]. \tag{61}$$

Fig. 4 also compares the predictions of the proposed model for the effective thermal conductivity (eqn. (56)) for the skin and the solid residue, left once the activity of chemical reactions and moisture evaporation are terminated, with the measurements reported in [28] over the temperature range 293–973 K. It should be noted that the parameter k_p (Table 2) is selected so as to get the same measured and simulated value of the effective thermal conductivity at 293 K. Also, the pore diameter, d, is evaluated requiring the coincidence of the simulated and measured effective thermal conductivity at 973 K, when conversion is already occurred. While the agreement between predictions and measurements is very good over a wide temperature range for the k_{eS} model proposed here, the apparent-value approach used in the empirical transport model [31] under-predicts the measured values at low temperature and highly overestimates those at high (>500 K) temperature.

The specific heat of the skin, c_S, is expressed as a mass averaged value of the specific heats of the polymer and fibre glass fractions:

$$c_S = \frac{\varepsilon_m \rho_m c_m + \varepsilon_p \rho_p c_p + \varepsilon_f \rho_f c_f + \varepsilon_g \rho_g c_g}{\varepsilon_m \rho_m + \varepsilon_p \rho_p + \varepsilon_f \rho_f + \varepsilon_g \rho_g}, \tag{62}$$

which, once the chemical reactions are completed, for the remaining part of the skin becomes

$$c_R = \frac{\varepsilon_p \rho_p c_p + \varepsilon_f \rho_f c_f + \varepsilon_g \rho_g c_g}{\varepsilon_p \rho_p + \varepsilon_f \rho_f + \varepsilon_g \rho_g}. \tag{63}$$

Table 2 lists the values of density and specific heat of each component. In particular, the latter parameters are assumed to be constant (the fibre glass value of 0.84 J/kgK is obtained from Ref. [41] for a temperature range 323–573 K). The comparison of the predictions of eqs. (62) and (63) with the experimental data [28] for a GRP skin, reported in Fig. 5, shows an acceptable agreement for both the skin and the final solid residue. On the contrary, the apparent specific heats used in the empirical transport model [31] are significantly different from the true physical values and appear to be not affected by the conversion process except for the effects of moisture evaporation (skin) simulated by a triangular dependence on temperature over the range 363–393 K.

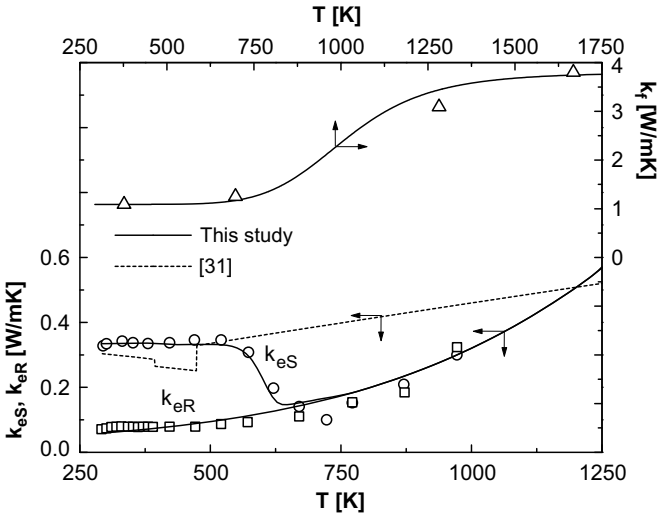

Fig. 4. Predictions of the skin effective thermal conductivity, k_{eS}, as given by eqn. (56) (solid line) and measurements [28] (squares and circles) as functions of temperature (the predictions of eqn. (61) (solid line) for the fibre thermal conductivity, k_f, and the measurements [46] (triangles) are also reported). The predictions of the skin effective thermal conductivity, k_{eS}, according to the formula used in [31] (dashed line) are included for comparison purposes.

The model for the effective thermal conductivity of the core also takes into account the contribution of the various components and a radiative term as:

$$k_{eC} = \varepsilon_{cs} k_{cs} + \varepsilon_m k_m + \varepsilon_g k_g + 4d \frac{\varepsilon_g}{1 - \varepsilon_g} \sigma e T^3. \tag{64}$$

The results of the k_{eC} model (eqn. (64)), in the absence of moisture, compare well with the experimental measurements reported in [47] for a calcium silicate board containing vermiculite, as shown on dependence of the temperature in Fig. 6. In addition to the main constituents, the density and the k_{cs} values at ambient temperature

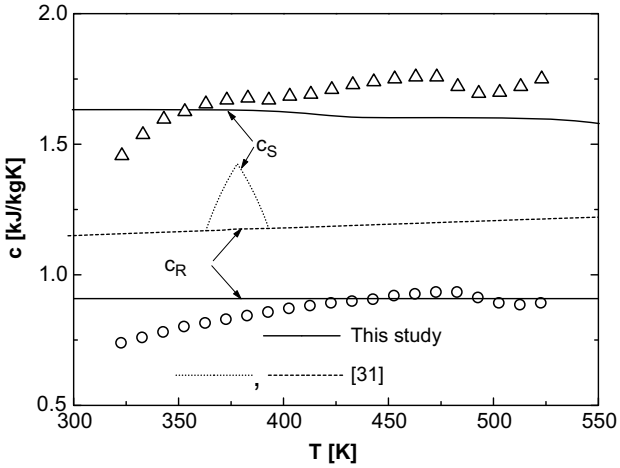

Fig. 5. Predictions of the specific heat for the skin (c_S, eqn. (62)) and the residue (c_R, eqn. (63)) (solid lines) and measurements [28] (squares and circles) as functions of temperature. The predictions of specific heat for the skin (dotted line) and the residue (dashed line) according to the formula used in [31] are included for comparison purposes.

are roughly coincident with those of Vermiculux supporting the validity of the proposed comparison. As expected, significant differences can be observed for the empirical expression of the core thermal conductivity used in [31].

The specific heat for the core, c_C, is expressed as a mass averaged value of the specific heats of the various components (parameter values again listed in Table 2):

$$c_C = \frac{\varepsilon_m \rho_m c_m + \varepsilon_{cs} \rho_{cs} c_{cs} + \varepsilon_g \rho_g c_g}{\varepsilon_m \rho_m + \varepsilon_{cs} \rho_{cs} + \varepsilon_g \rho_g}. \quad (65)$$

The experimental results reported in [47] are again used for comparison with the results of eqn. (65) for a dry material (Fig. 6). It can be seen that there is an acceptable agreement while the apparent specific heat expression used in [31] again presents large discrepancies. Similar to the skin case of Fig. 5, in the presence of moisture a triangular dependence appears on the temperature range 363–393 K.

The global heat transfer coefficients, h_1 and h_2, are computed from the correlation [48] for vertical slabs:

$$Nu = \left[0.825 + \frac{0.387 Ra^{1/6}}{\left(1 + \left(\frac{0.492}{Pr}\right)^{9/16}\right)^{8/27}} \right]^2, \quad (66)$$

where *Nu*, *Ra* and *Pr* are the Nusselt, Rayleigh and Prandtl numbers. All the properties are evaluated at the film temperature as mean values between the surface and the ambient temperature. The surface temperature is assumed to coincide with 1273 K for the computation of h_1 and 433 K (reference temperature for the standard test ISO834) for h_2. The lateral heat transfer coefficient h_L, is the average of the h_1 and h_2 values, where the former is modified to take into account the blowing effect [49]. The flame temperature, T_f, versus time profile, imposed at the external surface of the upper skin, is evaluated from the "hydrocarbon fire curve" [50]:

$$T_f = 293 + 1080\left(1 - 0.325e^{-0.0028t} - 0.675e^{-0.042t}\right). \quad (67)$$

Also, again in relation to the behaviour of the heat-exposed surface, the critical temperature, needed for surface ablation, T_{cr}, is taken equal to 1200 K (about 100 K higher than the glass fusion temperature). It should be noted that the external heating conditions are described by the hydrocarbon fire test curve defined according to the NPD standard [51] as used in the experiments [31,33,34] used to validate the model.

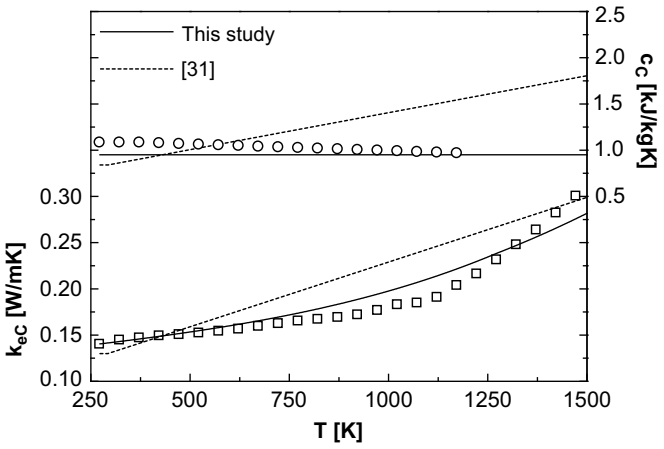

Fig. 6. Predictions of the dry core effective thermal conductivity, k_{eC} (eqn. (64)), and specific heat, c_C (eqn. (65)) (solid lines), and measurements as in [47] (squares and circles) as functions of temperature. The predictions of the dry core thermal conductivity and specific heat according to the formulae used in [31] (dashed line) are included for comparison purposes.

2.6. Numerical solution

The numerical solution of the system of differential equations with initial and boundary conditions is carried out in the framework of the software Matlab (version 6.3). Finite difference approximations are used for the spatial derivatives (first-order forward scheme for the convective terms and second-order space-centered scheme for heat conduction), so that the mathematical model is reduced to a system of ordinary differential equations. These are integrated with respect to the independent variable time by means of the routine ode15s. As soon as the temperature of the surface elementary cell, subjected to external heating, becomes higher than T_{cr}, the external boundary is displaced to the adjacent cell.

3. Results

Results are presented for the conversion dynamics of a single GRP panel ($L_{S1} = 1.09 \times 10^{-2}$ m, $H = 0.9$ m), using the experimental data reported in [33,34] for validation. Then results for the sandwich panel ($L_{S1} = L_{S2} = 9.6 \times 10^{-3}$ m, $L_C = 0.04$ m, $H = 0.9$ m) are produced. In this case the measurements reported in [31] are used for experimental validation. Time and space distributions of the main dependent variables are discussed as simulated using the kinetic parameters for the two-step model given in Table 1 and data listed in Table 2. Moreover the initial conditions are assigned as in the experiments used for validation: $T_0 = 293$ K, $\rho_{a0} = 1.2$ kg/m^3, $Y_{d0} = 0.571$, $Y_{c0} = 0.045$, $Y_{m0} = 0.001$ (skin), $Y_{m0} = 0.099$ (core). The numerical solution of the model equations is carried with a variable time step determined by a required accuracy level of the solution evaluated in terms of relative and absolute error by the routine ode15s of the software Matlab, assigned equal to 10^{-4} and 10^{-7}, respectively. The spatial grid comprises 80 cells for each skin and the core. These characteristics have been selected so as to obtain grid-independent solutions.

3.1. Single skin system

The main features of the thermal response of the composite-material skin can be observed from the spatial profiles at several times of temperature (Fig. 7), solid mass fraction and gas/vapor mass flux (Fig. 8), moisture evaporation rate (Fig. 9) and polyester decomposition and combustion rates (Fig. 10). As expected, the heating of the composite material takes place with significant spatial gradients. Moisture evaporation, in agreement with the experimental evidence, is a low-temperature process and, also owing to the very low content, is very rapid (it terminates at about 450 s). On the other hand, the thermal decomposition of the polymer is a much slower process and is responsible for the largest fraction of volatile produced. As already evident from the analysis of the thermogravimetric data, the combustion of the small amount of polymeric residue follows at even higher temperatures. As a consequence of the assumption of constant pressure, the volatile products generated from moisture evaporation and the chemical transformations of the polymeric component, flow only towards the heat-exposed surface.

Apart from the early initial heating transients for the still unreacted composite solid, the dynamics of the conversion process, as shown in Figs. 7–10, permit the introduction of three main temporal periods or conversion regimes. The first (times shorter

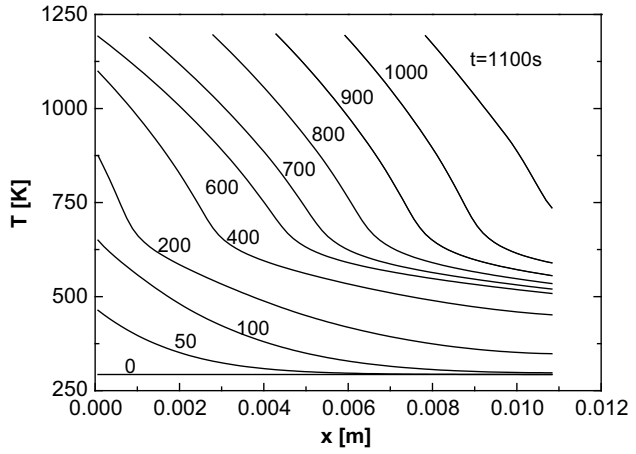

Fig. 7. Predicted temperature profiles along the single skin panel for several times.

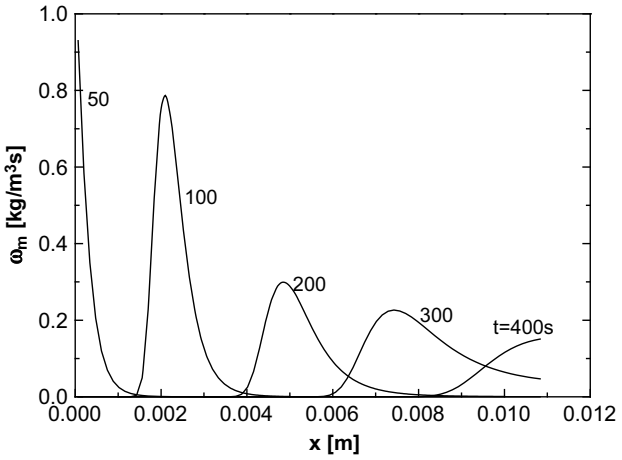

Fig. 9. Predicted profiles of the moisture evaporation rate along the single skin panel for several times.

than 200 s) is characterized by a thin surface region where chemical reactions are under way while a large part of the composite slab still presents properties at approximately the initial values (fast heating regime). The second period (times between 200 and 630 s) is characterized by the presence of a further spatial zone, where the release of volatile products is terminated and a low-density, inert zone consisting essentially of glass fibres extends up to the initial slab thickness (slow heating regime). Finally, for longer times (>630 s), the third period begins when part of the inert solid, left behind the chemical and physical transformations associated with volatile production, is ablated as a consequence of thermal softening and collapse of the glass fibres once temperatures above T_{cr} are attained (ablation regime).

For all the three regimes the wide zone, where thermal decomposition is under way, acts as an energy sink given its highly endothermic character. It separates a region of low, almost uniform temperature (unreacted composite material) from one of high temperature with large spatial gradients (essentially the region of inert, already reacted material, since the amount of solid interested by exothermic combustion is small). From the qualitative point of view, the mass flux which, for each spatial position, takes into account the variations in the total gas density and the total amount of volatile produced (from the bottom up to the selected spatial position), presents slowly increasing values along the evaporation zone, a rapid rise along the degradation zone and, finally, a further small increase along the combustion zone. For the inert already reacted zone, the volatile mass flux remains constant at the maximum value indicating that, at least for this zone, the effects of total density variation are small.

The temperature profiles along the reacting slab, and consequently the rate of moisture evaporation and the activity of chemical reactions, are highly influenced by the distance of the reacting/evaporation zone from the heat-exposed surface. These effects can be clearly seen from the position of the ablation front (Fig. 11) and the positions (Fig. 11) and corresponding values (Fig. 12) of the maxima of the evaporation, thermal degradation and combustion rates as functions of time. Given the short duration compared with that of chemical conversion, moisture evaporation is not influenced by surface ablation. The maximum evaporation rate, apart from the early peak, continuously decreases owing to the successively longer distance from the heated surface (Figs. 9 and 12), but the propagation speed of the maximum (Fig. 11), after the initial decrease, starts to increase again ($t > 200$ s) as a consequence of the enlargement in the size of the evaporation zone (Fig. 9) up to the entire slab thickness.

Chemical conversion for the fast heating regime is also quite rapid for a thin superficial layer where chemical and physical transformations occur at high temperatures (high maximum rates). The highest propagation speeds of the maximum decomposition

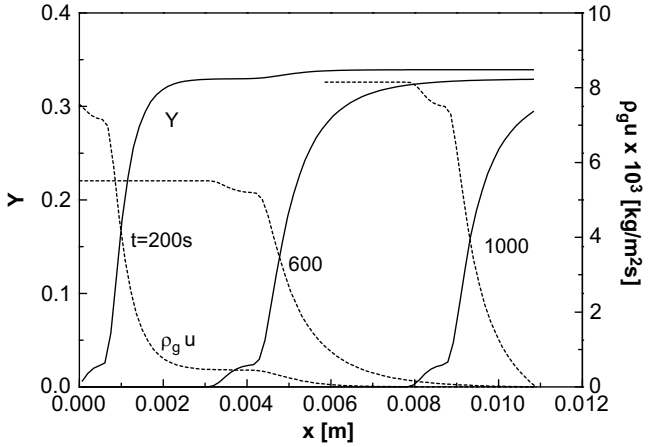

Fig. 8. Predicted profiles of condensed-phase mass fraction (solid lines) and volatile mass flux (dashed lines) along the single skin panel for several times.

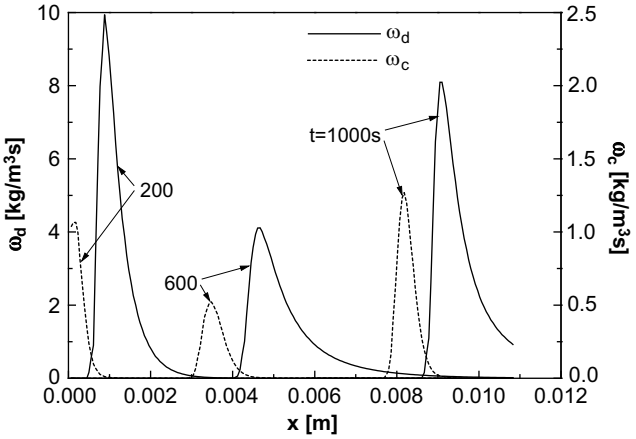

Fig. 10. Predicted profiles of the decomposition (solid lines) and combustion (dashed lines) rates along the single skin panel for several times.

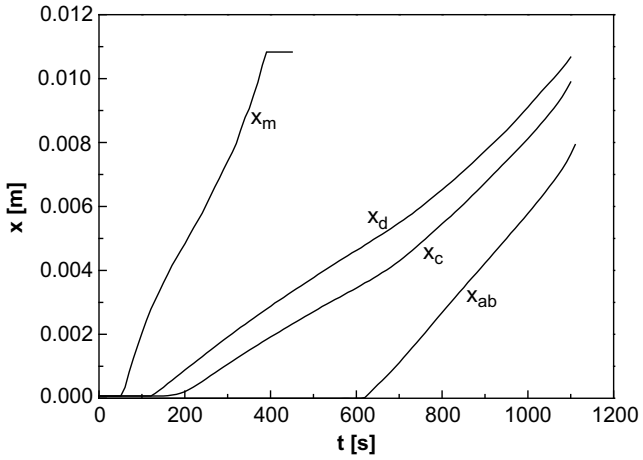

Fig. 11. Predicted positions of the maximum of moisture evaporation (x_m), thermal decomposition (x_p) and combustion (x_c) rate and position of the ablation front (x_{ab}) versus time for the single skin panel.

and combustion rates are attained at about 200 and 240 s, respectively (Fig. 11). Then, for the second regime of slow heating, the formation of a low thermal conductivity and already reacted solid layer makes difficult the heat transfer from the external flame to the reaction zone: volatile formation takes place at lower temperatures with reduced rates (see the continuously decreasing maximum value, Figs. 10 and 12) which results in a strong reduction in the total mass flow rate across the porous solid (Fig. 8). The propagation speeds of the maximum decomposition and combustion rate also present slightly decreasing values (Fig. 11). The low thermal conductivity of the upper already reacted solid favors the rise of the surface temperature until a critical value is attained with the consequent ablation of the surface (times longer than 630 s). The reduction in the thickness of the already reacted solid causes an increase in the rate of inward heat transfer with an enhancement in the rates of volatile species production (Fig. 12) and in the total gas/vapor mass flux. Thus, the third period (ablation regime) is characterized by a new increase in the propagation speed of the maximum reaction rates which, for times longer than 900 s, become roughly the same or higher than those of the initial period (Fig. 11). It can be expected that, for the ablation regime, a quasi-steady behaviour for the propagation rates of the ablation front and the maxima in the evaporation and reaction rates could be established given sufficiently thick slabs. On the other hand, it can be observed that the propagation speed of the ablation front is already approximately constant as long as the effects of the bottom boundary are small (times shorter than 1000 s).

The comparison between the predicted and measured [33,34] temperature versus time profiles at three different slab heights shows a good agreement (Fig. 13), supporting the validity of the model developed and the correct selection of the input data used for the simulation. The model predicts well the plateau at about 625 K for the first two more external positions, that can be attributed to the local endothermicity of the thermal decomposition reaction (measurements for the position $x = L_{S1}$ are at times too short for the beginning of this reaction). The delay in the temperature rise measured at $x = L_{S1}/2$ and $x = L_{S1}$ at lower temperatures can again be attributed to the energetics of thermal decomposition occurring at the above layer. Apart from the small content, the effects of moisture evaporation are not clearly evident from both the measured and predicted shape of the temperature profiles, presumably because of the fast heating rates and the large spatial gradients.

The results of the empirical model [33] are also included in Fig. 13 for comparison. Although the comparison between predictions and experiments is also acceptable, it should be kept in mind that the empirical model, apart from the numerous simplifications in the description of chemical and physical processes, is based on apparent values of the most important properties, i.e. kinetic parameters (Fig. 3), effective specific heats and thermal conductivities (Figs. 4–6) which are used, in some way, as adjustable parameters to obtain the best fit between model predictions and measurements. On the contrary, the model proposed here makes use of intrinsic property values and considers an explicit description of the main chemical and physical processes for the system of interest. Therefore it offers a sound basis for further extension to different operating conditions and/or materials.

3.2. Sandwich panel

The temperature profiles along the sandwich panel, as simulated for several times, are reported in Fig. 14 (solid lines). For comparison purposes the profiles along the upper skin, as simulated for the case of the single skin panel, are also shown (dashed lines). It can be seen that these are not significantly affected by the multi-layer features of the sandwich. Heat transmission across the

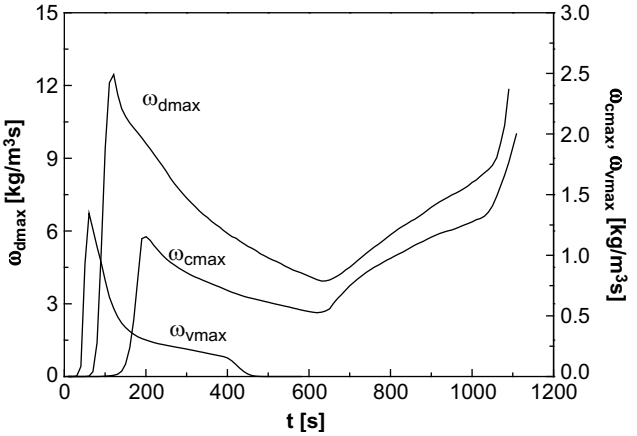

Fig. 12. Maximum rates of moisture evaporation, polymer decomposition and combustion versus time for the single skin panel.

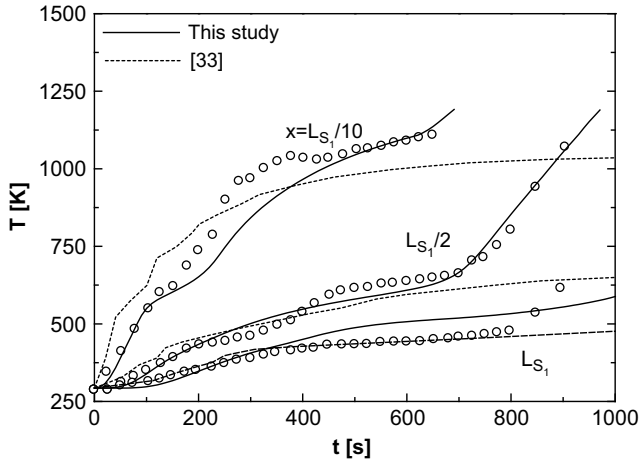

Fig. 13. Predicted (solid lines) and measured ([33,34], symbols) temperatures versus time profiles at three spatial positions of the single skin panel. The predictions obtained by the model [33] (dashed lines) are included for comparison purposes.

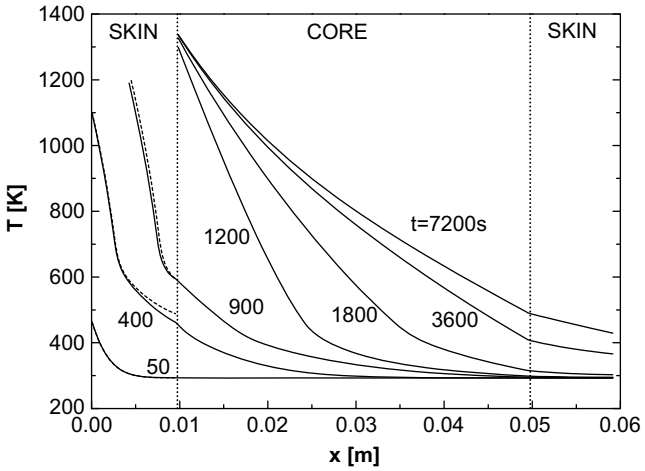

Fig. 14. Predicted temperature profiles along the sandwich (solid lines) and single skin (dashed lines) panels for several times.

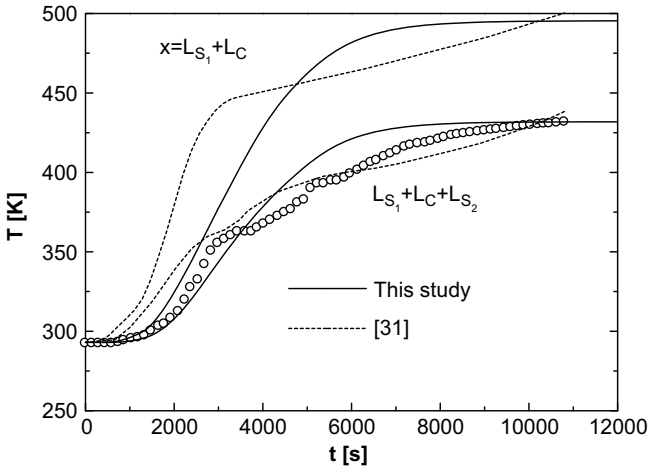

Fig. 16. Predicted (solid lines) and measured ([31], symbols) temperature versus time profiles at two spatial positions of the sandwich panel. The predictions by the model [31] (dashed lines) are included for comparison purposes.

core is a quite slow process, owing to its lower effective thermal conductivity, especially for the first two conversion regimes of the upper skin when the surface temperature remains below the value T_{cr}. The spatial profiles of the moisture evaporation rate (Fig. 15), the sole conversion process taking place along the core, show maximum values and propagation speeds of the evaporation region that are initially (first two conversion regimes of the upper skin) successively reduced. Then, as a consequence of the complete ablation of the upper skin, an absolute maximum is reached (at about 1200 s), followed by a reduction in the progress of moisture evaporation as a consequence of the successively thicker layer of already dried and low-conducting core. Although complete drying of the core and the lower skin can be observed for about 3600 s, a steady temperature profile is attained only for times longer than about 7200 s. It can be noted that the lower skin always remains at temperatures too low for any chemical transformation.

The comparison between the measured [31] and the simulated temperature versus time profiles at the cold bottom of the sandwich panel shows good agreement (Fig. 16). The temperature starts to rise for times longer than 2000 s when the upper skin does not exist any more. Therefore the dynamics of the heat-exposed skin affect the bottom side of the sandwich panel only indirectly through the variations caused in the thermal profiles along the core. For times of about 3000 s, the measured profile shows a plateau around 373 K, the atmospheric water boiling point. It is likely that moisture evaporation takes place simultaneously along the entire thickness of the skin given the very slow heating rates and the reduced spatial gradients. However, the Arrhenius rate of moisture evaporation employed by the model does not describe well this feature and consequently a slightly faster temperature rise is predicted. Also, as already observed from the spatial profiles, it can be seen that the smaller the distance from heated surface the shorter the time for steady conditions and the higher the steady temperature value. Finally, the comparison between measurements and simulations of the model [31] shown in Fig. 16 is also acceptable but this model presents the drawbacks already discussed for the single skin panel.

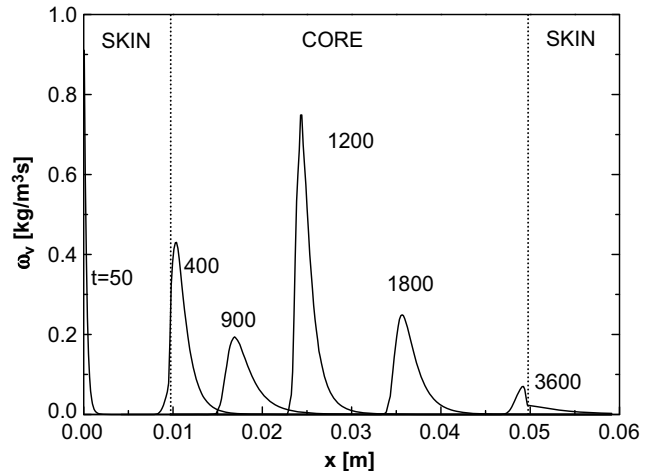

Fig. 15. Predicted profiles of the moisture evaporation rate along the sandwich panel for several times.

4. Conclusions

Despite the great industrial importance of the thermal response of sandwich panels exposed to fire and the widely acknowledged usefulness of mathematical modelling for the determination of the controlling mechanisms needed for material/structure design, a brief review of the literature shows that current predictions of the process dynamics are based only on a purely empirical approach. Indeed, the model [31] for a GRP–Vermiculux sandwich, apart from the simplifications in the formulation of the differential equations, makes use of apparent specific heats and thermal conductivities and guessed chemical kinetics for a single assigned condition. In this way, the effects cannot be predicted, as caused by modifications in the fire exposure conditions and/or size and properties of the sample. Hence a significant advancement in the state of the art is represented by the model developed and experimentally validated in this study. It is a predictive comprehensive model, based on a rigorous formulation of the conservation equations and the use of intrinsic chemical and physical properties, for multi-layered systems subjected to fire that, in principle, can be applied to a variety of practical situations by simply varying the input data. The multi-layered system used here is the same as in [31]. In addition to the obvious implications from the practical side, this system has been selected because experimental measurements are available for the most important physical properties and the weight loss characteristics of the polymeric component of the skin, that can be used for the development of reliable sub-models to be coupled with transport equations, and for the temperatures of the

single skin and sandwich panels, that can be used for the experimental validation of the comprehensive model.

Thus weight loss data of isophthalic polyester (the polymeric compound of the skins) in air have been interpreted by a kinetic mechanism consisting of a first-order decomposition reaction and an *n*-order combustion reaction both with an Arrhenius-type dependence on temperature giving activation energies of 128 and 150 kJ/mol, respectively. Also models have been proposed and validated for the effective thermal conductivities and specific heats of the composite materials constituting the skins and the core of the sandwich panel. The kinetic model and the sub-models for the physical properties have been coupled with the unsteady, one-dimensional conservation equations taking into account heat transfer by convection and conduction, convective mass transfer, surface heat transfer, moisture evaporation, and ablation of the heat-exposed surface at a critical temperature.

The agreement between measured and predicted temperature versus time profiles for the composite skin and the sandwich panel is good without any modification in the intrinsic chemico-physical properties. Moreover, it has been found that the dynamic behaviour of the sandwich panel is largely determined by the heat-exposed skin. This undergoes three main regimes: I) very rapid conversion of a thin surface layer, II) slowing down of the conversion processes following the formation of a thick insulating fibre glass layer and III) a new enhancement in the reaction rates as a consequence of surface collapse and ablation. However, as the experimental validation is limited to only a single case for both the skin panel and the multi-layered sandwich structure, it is highly desirable that in a near future more experimental data will be made available to strengthen the evidence of the general validity of the proposed model.

The successive applications of the comprehensive model presented and experimentally validated here should also investigate the model sensitivity to the assumptions made in the description of the various processes and parameter values. In particular, the effects of the uncertainty in the boundary conditions at the heat-exposed surface should be ascertained given the prominent role played by the external heating intensity and modality on the thermal response of the material. Other aspects to be investigated concern, for instance, the role of thermal and oxidative decomposition of the polymeric resin, moisture evaporation and the model for the effective thermal conductivity of the material. Results could help in the development of reliable simplified models that can be extended to include structural effects and/or can be used in conjunction with computational fluid dynamics tools to simulate a large-scale fire scenario. A parametric analysis could also be particularly useful to evaluate the influence of the sandwich characteristics on the fire response. Finally, the proposed transport model could be the basis for further development and simulation of sandwich systems based on different materials.

Acknowledgments

This work is part of the activities carried out in the framework of the project PIROS "Progettazione integrata di componenti mltifunzionali per applicazioni in sistemi del settore ferrotranviario e dei vettori di medie dimensioni, associata alla realizzazione di speciali facilities per prove e qualificazioni di materiali in condizioni di fiamma", coordinated by IMAST and funded by the Italian Ministry of Instruction, University and Research (MIUR), the partial support of which is gratefully acknowledged. C. Di Blasi and A. Galgano also express their sincere appreciation for the enthusiastic contribution given by Roberta Papale and Costanzo Vellino during the initial stage of this work.

References

[1] Heimbs S, Schmeer S, Middendorf P, Maier M. Strain rate in phenolic composites and phenolic-impregnated honeycomb structures. Compos Sci Technol 2007;67:2827–37.
[2] Mouritz AP, Gardiner CP. Compression properties of fire-damaged polymer sandwich composites. Compos Part A Appl Sci 2002;33:609–20.
[3] Bozhevolnaya E, Lyckegaard A. Structurally graded core inserts in sandwich panels. Compos Struct 2005;68:23–9.
[4] Vaidya AS, Vaidya UK, Uddin N. Impact response of three-dimensional multifunctional sandwich composite. Mater Sci Eng A Struct 2008;472:52–8.
[5] Dodds N, Gibson AG, Dewhurst D, Davies JM. Fire behavior of composite laminates. Compos Part A Appl Sci 2000;31:689–702.
[6] Henderson JB, Wiebelt JA, Tant MR. A model for the thermal response of polymer composite materials with experimental verification. J Compos Mater 1985;19:579–95.
[7] Florio J, Henderson JB, Test FL, Hariharan R. A study of the effects of the assumption of local-thermal equilibrium on the overall thermally-induced response of a decomposing, glass-filled polymer composite. Int J Heat Mass Transfer 1991;34:135–47.
[8] Di Blasi C, Wichman IS. Effects of solid phase properties on flames spreading over composite materials. Combust Flame 1995;102:229–40.
[9] Di Blasi C. Modeling of solid and gas phase processes during composite material degradation. Polym Degrad Stab 1996;54:241–8.
[10] Di Blasi C. Modeling the effects of high radiative heat fluxes on intumescent material decomposition. J Anal Appl Pyrol 2004;71:721–37.
[11] Nelson MI, Brindley J, McIntosh AC. Ignition of thermally thin thermoplastics – the effectiveness of inert additives in reducing flammability. Polym Degrad Stab 1996;54:255–66.
[12] Staggs JEJ. A simplified mathematical model for the pyrolysis of polymers with inert additives. Fire Safety J 1999;32:221–40.
[13] Staggs JEJ. Modeling the effect of solid-phase additives on thermal degradation of solids. Polym Degrad Stab 1999;64:369–77.
[14] Di Blasi C, Branca C. A mathematical model for the non-steady decomposition of intumescent coatings. AIChE J 2001;47:2359–70.
[15] Neininger SM, Staggs JEJ, Horrock AR, Hill NJ. A study of the global kinetics of thermal degradation of a fibre-intumescent mixture. Polym Degrad Stab 2002;77:187–94.
[16] Branca C, Di Blasi C, Horacek H. Analysis of the combustion kinetics and the thermal behavior of an intumescent system. Ind Eng Chem Res 2002;41:2104–14.
[17] Lua J, O'Brien J, Key CT, Wu Y, Lattimer BY. A temperature and mass dependent thermal model for fire response prediction of marine composites. Compos Part A Appl Sci 2006;37:1024–39.
[18] http://code.google.com/p/gpyro.
[19] Mouritz AP, Gibson AG. Fire properties of polymer composite materials. Dordrecht: Springer; 2006.
[20] Di Blasi C. Modeling and simulation of combustion processes of charring and non-charring solid fuels. Prog Energ Combust 1993;19:71–104.
[21] Di Blasi C. The state of the art of transport models for charring solid degradation. Polym Int 2000;49:1133–46.
[22] Di Blasi C. Modeling chemical and physical processes of wood and biomass pyrolysis. Prog Energ Combust 2008;34:47–90.
[23] Staggs JEJ. Heat and mass transport in developing chars. Polym Degrad Stab 2003;82:297–307.
[24] Lattimer BY, Oullette J. Properties of composite materials for thermal analysis involving fires. Compos Part A Appl Sci 2006;37:1068–81.
[25] Keller T, Tracy C, Zhou A. Structural response of liquid-cooled GFRP slabs subjected to fire – Part I: material and post-fire modeling. Compos Part A Appl Sci 2006;37:1286–95.
[26] Keller T, Tracy C, Zhou A. Structural response of liquid-cooled GFRP slabs subjected to fire – part II: thermo-chemical and thermo-mechanical model. Compos Part A Appl Sci 2006;37:1296–308.
[27] Bai Y, Vallée T, Keller T. Modeling of thermo-physical properties for FRP composites under elevated and high temperature. Compos Sci Technol 2007;67:3098–109.
[28] Bai Y, Post NL, Lesko JJ, Keller T. Experimental investigations on temperature-dependent thermo-physical and mechanical properties of pultruted GFRP composites. Thermochim Acta 2008;469:28–35.
[29] Feih S, Mathys Z, Gibson AG, Mouritz AP. Modeling the tension and compression strengths of polymer laminates in fire. Compos Sci Technol 2007;67:551–64.
[30] Feih S, Mathys Z, Gibson AG, Mouritz AP. Modeling the compression strength of polymer laminates in fire. Compos Part A Appl Sci 2007;38:2354–65.
[31] Looyeh MRE, Rados K, Bettess P. Thermochemical responses of sandwich panels to fire. Finite Elem Anal Des 2001;37:913–27.
[32] Looyeh MRE, Rados K, Bettess P. A one-dimensional finite element simulation for the fire-performance of GRP panels for offshore structures. Int J Numer Methods Heat Fluid Flow 1997;7:609–25.
[33] Looyeh MRE, Bettess P. A finite element model for the fire performance of GRP panels including variable thermal properties. Finite Elem Anal Des 1998;30:313–24.
[34] Krysl P, Ramroth WT, Srewart LK, Asaro RJ. Finite element modeling of fibre reinforced polymer sandwich panels exposed to heat. Int J Numer Methods Eng 2004;61:49–68.

[35] Looyeh MRE, Samanta A, Jihan S, McConnachie J. Modeling of reinforced polymer composites subject to thermo-mechanical loading. Int J Numer Methods Eng 2005;63:898–925.
[36] www.promat.co.uk/fp-products-vermiculux.htm.
[37] Branca C, Di Blasi C. Devolatilization and combustion kinetics of wood chars. Energ Fuels 2003;17:1609–15.
[38] Perry RH, Green DW, Maloney JO, editors. Perry's chemical engineers' handbook. 6th ed. New York: McGraw-Hill; 1984.
[39] Di Blasi C, Branca C, Sparano S, La Mantia B. Drying characteristics of wood cylinders for conditions pertinent to fixed-bed countercurrent gasification. Biomass Bioenerg 2003;25:45–58.
[40] Gronli MG. A theoretical and experimental study of the thermal degradation of biomass. PhD thesis, Trondheim, Norway: NTNU; 1996.
[41] Drysdale D. An introduction to fire dynamics. New York (NY): John Wiley & Sons, Inc; 1998.
[42] Turner IW, Puiggali JR, Jomaa W. A numerical investigation of combined microwave and convective drying of a hygroscopic porous material: a study based on pine wood. Trans IchemE Part A 1998;76:193–209.
[43] Di Blasi C. Dynamic behaviour of stratified downdraft gasifiers. Chem Eng Sci 2000;21:2931–44.
[44] Galgano A, Di Blasi C. Modeling wood degradation by the unreacted-core-shrinking approximation. Ind Eng Chem Res 2003;42:2101–11.
[45] Larfeldt J. Drying and pyrolysis of logs of wood, PhD thesis, Göteborg, Sweden: Department of Energy Conversion, Chalmers Teknisks Hogskola; 2000.
[46] Jacoutot L, Fautrelle Y, Gagnoud A, Brun Lacombe J. Numerical modeling of coupled phenomena in a mechanically stirred molten-glass bath heated by induction. Chem Eng Sci 2008;63:2391–401.
[47] www.eaa.net/eaa/education/TALAT/lectures2502.pdf.
[48] Churchill SW, Chu HHS. Correlating equations for laminar and turbulent free convection from a vertical plate. Int J Heat Mass Transfer 1975;18:1323–9.
[49] Sherwood TK, Pigford RL, Wilke CR. Mass transfer. New York: McGraw-Hill; 1975.
[50] EC 1. Eurocode 1: actions on structures. ENV 1991, Part 1–2: general actions – actions on structures exposed to fire. Brussels: European Committee for Standardization; 2002.
[51] Gibson AG, Wu Y-S, Chandler HW, Wilcox JAD, Bettess P. A model for the thermal performance of thick composite laminates in hydrocarbon fires. Rev L'Inst Fr Pet 1995;50:69–74.